Utilization of Region-wise Even-Parity Discontinuity Factor to Reduce
Discretization Error of MOC

Akio YAMAMOYO[*], Akinori GIHO, Tomohiro ENDO[*]

*) Graduate School of Engineering, Nagoya University

Corresponding author: Akio YAMAMOTO

E-mail: a-yamamoto@energy.nagoya-u.ac.jp

Address: Nagoya University, Furo-cho, Chikusa-ku, Nagoya, Japan, 464-8603

Tel, Fax: +81-52-789-5121, +81-52-789-3606

Number of Pages: 16

Number of Tables: 3

Number of Figures: 9

ABSTRACT

To reduce angular and spatial discretization error of MOC with a coarse calculation condition, the region-wise even-parity discontinuity factor (EPDF) for transport calculations is evaluated through an iterative procedure using only region-wise scalar flux, i.e., without odd parity angular flux, partial-, or net-current at region boundary. Region-wise EPDF is evaluated in a single assembly geometry with reflective boundary condition. The evaluated EPDF are applied to 2x2 colorset assembly and core configurations and the performance is compared to that of the conventional superhomogenization (SPH) method. The calculation results indicate that 1) no convergence issue is observed during the iteration process to estimate EPDF, 2) performance of the region-wise EPDF is better than that of the conventional SPH method, 3) the normalization of EPDF is necessary to incorporate different surface scalar flux levels among different types of fuel assemblies.

2

I. INTRODUCTION

The Method of Characteristics (MOC) has been widely used not only for lattice physics calculations, but also for whole core analyses. In the case of lattice physics computation, the use of fine energy group (*e.g.*, a few hundred), fine quadrature set (*e.g.*, a hundred for azimuthal, 3 for polar), and fine ray trace (*e.g.*, 0.05cm) is practical and can be used for production calculations.

Application of MOC to whole core analyses is being practical by utilization of the planar MOC method and various advanced core analysis codes have been developed [1]-[6]. The planar MOC method greatly improves the computational efficiency of three-dimensional whole core calculations with explicit heterogeneous geometry, but the application of the fine calculation condition used in lattice physics calculations still requires very large computational cost and cannot be carried out with affordable PCs. The latest supercomputer would be necessary to meet such large computational requirements. Therefore, the use of a coarser calculation condition is necessary for practical calculations when a three-dimensional heterogeneous transport method is used. This fact implies that a mitigation measure for angular, spatial, and energetic discretization error is still necessary for the latest core simulations. Namely, a correction method is required for a coarse calculation to accurately reproduce the result of a fine calculation.

The superhomogenization (SPH) method is a well-known correction method used to reduce errors due to various approximations in calculations [7]-[9]. The SPH method has been extensively used for diffusion and SP_N pin-by-pin fine mesh core calculations in which the cell homogenization error should be reduced [7]-[10]. The SPH method is also applied to reduce energy collapsing error in a resonance calculation, in which reaction rate obtained by an ultra-fine group calculation is preserved in a multi-group calculation using the SPH factor [11][12]. The SPH method is a generic correction method and can be used for various applications. Thus, the application of the SPH method to correct errors of MOC due to a coarse calculation condition seems to be straightforward. In fact, the SPH method can successfully reduce the discretization error of MOC in many cases. However, the SPH method with MOC may fail to evaluate appropriate correction factor especially when strong absorber exists in a small part of calculation geometry, *e.g.*, Gd bearing fuel pellet with subdivision or control rod absorber. The SPH method has another deficiency in that the neutron partial currents are not explicitly preserved at each region boundary. Thus, degradation of accuracy tends to be larger when the boundary condition is changed.

An alternate approach for correction is the discontinuity factor (DF). The DF is widely used in the field of core analysis with advanced nodal methods based on the diffusion theory [13]-[15]. In principle, the DF can be used not only with the diffusion theory, but also with the transport theory. However, the application of DF to the transport theory is rather complicated compared to that of the diffusion theory, and therefore has not been widely adopted. For example, the tally of angular flux (or angular flux moments) is

necessary at each surface of the flux region to rigorously estimate DF for angular flux [16]. This complicated process would be an obstacle for the practical utilization of DF with MOC. Note that partial currents or angular flux can be explicitly preserved with DF, thus the degradation of accuracy is smaller than that of SPH when the boundary condition is changed.

In the present paper, a new iteration procedure to estimate the region-wise DF for MOC without the information of angular flux, partial- or net-current at each surface of the flux region is described. Only the region average scalar flux is used in the present method. This procedure is equivalent to that used to obtain the conventional SPH factors. The DFs are estimated in a single assembly geometry with the reflective boundary condition. The performance of DF to mitigate the discretization error of MOC with a coarse calculation condition is compared with that of the SPH method in colorset and core geometries.

It should be noted that the region-wise DF and the SPH factor are equivalent in the diffusion and transport theory using the second order differential form, but they are different in the transport theory using the first order differential form (e.g., Sn, MOC) as discussed in section II.A. This is a key point of the present study.

The remaining part of this paper is organized as follows. In section II, the theoretical descriptions for evaluation of DF using an iteration procedure are given. Performance comparison of DF and SPH is shown in section III. Finally, concluding remarks are summarized in section IV.

II. THEORY AND CALCULATION PROCEDURES

II.A. Definition of DF in This Study and Relation with SPH factor

Various DFs have been proposed for the transport theory. They are classified into the angular flux discontinuity factor (AFDF) [16], [17], the partial current discontinuity factor (PCDF) [15], [18] and the even parity angular flux discontinuity factor (EPDF) [19], [20]. The AFDF and the PCDF directly apply the discontinuity factor to angular flux while the EPDF applies the discontinuity factor to the even parity angular flux. In the present study, the EPDF is utilized among them. The reason for this choice is described as follows.

To estimate AFDF or PCDF, the tally of angular flux or partial current is necessary for all surfaces of all flux regions as described in Refs.[16] and [18]. Tally and storage of these parameters require considerable computational time and memory storage, especially in the case of AFDF, which has angular dependence. In many MOC code, the net or partial current is tallied at fuel cell boundary for acceleration, but AFDF and PCDF require the angular flux or the partial current at all surfaces of all flux regions, for which additional implementation work is necessary. The next point is conservation of neutron balance.

Since angular fluxes are discontinuous, the net current directly calculated by the discontinuous angular fluxes can be also discontinuous. This requires careful treatment of neutron balance in implementation, for example, the net neutron current directly calculated by the discontinuous angular flux cannot be used for an acceleration calculation by the coarse mesh finite difference (CMFD) or the generalized coarse mesh rebalance (GCMR) methods.

In the EPDF, the discontinuity factor is applied to the even parity angular flux and the continuity condition is applied to the odd parity angular flux. This concept is a straightforward extension of the conventional DF for diffusion theory. Since continuity of all odd parity angular fluxes is guaranteed with EPDF, neutron net current at any surface, which is obtained by angular integration of the odd parity angular flux multiplied by the direction cosine, is continuous even if angular flux itself is discontinuous. Thus, neutron balance for even-parity angular flux (thus scalar flux) is always conserved even if the calculated angular flux is directly used.

To estimate the surface-dependent EPDF, the even and odd parity angular fluxes at region surface are necessary. By forcing the odd parity angular fluxes obtained by a reference calculation as the boundary condition, the even parity angular fluxes at boundaries are estimated by solving the transport equation of second order differential form in each flux region. Once the even parity angular flux at the boundary is obtained, the EPDF is estimated by the ratio of the reference even parity angular flux over the estimated even parity angular flux. This is the same procedure to estimate DF in the diffusion theory.

In the case of surface-dependent EPDF, the even and odd parity angular fluxes are necessary at all surfaces of all flux regions, which is equivalent to AFDF. However, in the case of region-wise EPDF, the even and odd parity angular fluxes at boundaries are not necessary. Thus, the region-wise EPDF is considered in the present study due to computational efficiency.

To discuss the relationship between the region-wise EPDF and the SPH factor, let us consider a one-group, even-parity transport equation [21] in a two-region, one-dimensional slab geometry with isotropic scattering and reflective boundary.

$$
\begin{aligned}
-\frac{\mu^2}{\Sigma_{t,L}} \frac{d^2 \psi_L^e(x,\mu)}{dx^2} + \Sigma_{t,L} \psi_L^e(x,\mu) &= \frac{1}{2}\left(\left(\frac{\nu\Sigma_{f,L}}{k} + \Sigma_{s,L}\right) \int_{-1}^{1} \psi_L^e(x,\mu) d\mu\right), \\
-\frac{\mu^2}{\Sigma_{t,R}} \frac{d^2 \psi_R^e(x,\mu)}{dx^2} + \Sigma_{t,R} \psi_R^e(x,\mu) &= \frac{1}{2}\left(\left(\frac{\nu\Sigma_{f,R}}{k} + \Sigma_{s,R}\right) \int_{-1}^{1} \psi_R^e(x,\mu) d\mu\right),
\end{aligned}
\tag{1}
$$

where μ, ψ^e, and x are the cosine direction of neutron flight direction, the even-parity angular flux, and the coordinate, respectively. The subscripts L and R indicate the left and the right regions in the two-region problem, respectively. Other notations are conventional ones.

Equation (1) is solved with the following boundary conditions:

$$\psi_L^e(0,\mu) = \psi_R^e(0,\mu),$$

$$-\frac{1}{\Sigma_{t,L}}\frac{d\psi_L^e(0,\mu)}{dx} = -\frac{1}{\Sigma_{t,R}}\frac{d\psi_R^e(0,\mu)}{dx},$$

$$-\frac{1}{\Sigma_{t,L}}\frac{d\psi_L^e\left(-\frac{a}{2},\mu\right)}{dx} = -\frac{1}{\Sigma_{t,R}}\frac{d\psi_R^e\left(+\frac{a}{2},\mu\right)}{dx} = 0. \tag{2}$$

Note that the origin of coordinate is set at the boundary between the left and right regions, and each region has the same thickness of $a/2$.

The SPH method is applied to Eq.(1) by multiplying the SPH factors for the left and the right regions ($1/f_L$ and $1/f_R$) to the cross sections. Note that $1/\Sigma_t$ corresponds to the diffusion coefficient thus the SPH factor is multiplied to $1/\Sigma_t$.

$$-\frac{\mu^2}{f_L\Sigma_{t,L}}\frac{d^2\psi_L^e(x,\mu)}{dx^2} + \frac{\Sigma_{t,L}}{f_L}\psi_L^e(x,\mu) = \frac{1}{2}\left(\left(\frac{\nu\Sigma_{f,L}}{f_L k} + \frac{\Sigma_{s,L}}{f_L}\right)\int_{-1}^{1}\psi_L^e(x,\mu)d\mu\right),$$

$$-\frac{\mu^2}{f_R\Sigma_{t,R}}\frac{d^2\psi_R^e(x,\mu)}{dx^2} + \frac{\Sigma_{t,R}}{f_R}\psi_R^e(x,\mu) = \frac{1}{2}\left(\left(\frac{\nu\Sigma_{f,R}}{f_R k} + \frac{\Sigma_{s,R}}{f_R}\right)\int_{-1}^{1}\psi_R^e(x,\mu)d\mu\right). \tag{3}$$

The boundary conditions are:

$$\psi_L^e(0,\mu) = \psi_R^e(0,\mu),$$

$$-\frac{1}{f_L\Sigma_{t,L}}\frac{d\psi_L^e(0,\mu)}{dx} = -\frac{1}{f_R\Sigma_{t,R}}\frac{d\psi_R^e(0,\mu)}{dx},$$

$$-\frac{1}{f_L\Sigma_{t,L}}\frac{d\psi_L^e\left(-\frac{a}{2},\mu\right)}{dx} = -\frac{1}{f_R\Sigma_{t,R}}\frac{d\psi_R^e\left(+\frac{a}{2},\mu\right)}{dx} = 0. \tag{4}$$

Now we consider the following even-parity angular fluxes:

$$\tilde{\psi}_L^e(x,\mu) \equiv \frac{\psi_L^e(x,\mu)}{f_L},$$

$$\tilde{\psi}_R^e(x,\mu) \equiv \frac{\psi_R^e(x,\mu)}{f_R}. \tag{5}$$

By substituting Eq.(5) into Eq.(3), the following equations are obtained:

$$-\frac{\mu^2}{\Sigma_{t,L}}\frac{d^2\tilde{\psi}_L^e(x,\mu)}{dx^2} + \Sigma_{t,L}\tilde{\psi}_L^e(x,\mu) = \frac{1}{2}\left(\left(\frac{\nu\Sigma_{f,L}}{k} + \Sigma_{s,L}\right)\int_{-1}^{1}\tilde{\psi}_L^e(x,\mu)d\mu\right),$$

$$-\frac{\mu^2}{\Sigma_{t,R}}\frac{d^2\tilde{\psi}_R^e(x,\mu)}{dx^2} + \Sigma_{t,R}\tilde{\psi}_R^e(x,\mu) = \frac{1}{2}\left(\left(\frac{\nu\Sigma_{f,R}}{k} + \Sigma_{s,R}\right)\int_{-1}^{1}\tilde{\psi}_R^e(x,\mu)d\mu\right). \tag{6}$$

Similarly, by substituting Eq.(5) into Eq.(4), the following boundary conditions are obtained:

$$f_L\tilde{\psi}_L^e(0,\mu) = f_R\tilde{\psi}_R^e(0,\mu), \tag{7}$$

$$-\frac{1}{\Sigma_{t,L}}\frac{d\tilde{\psi}_L^e(0,\mu)}{dx} = -\frac{1}{\Sigma_{t,R}}\frac{d\tilde{\psi}_R^e(0,\mu)}{dx},$$

$$-\frac{1}{\Sigma_{t,L}}\frac{d\tilde{\psi}_L^e\left(-\frac{a}{2},\mu\right)}{dx} = -\frac{1}{\Sigma_{t,R}}\frac{d\tilde{\psi}_R^e\left(+\frac{a}{2},\mu\right)}{dx} = 0.$$

Equations (6) and (7) indicate the even-parity transport equation with the discontinuity factor for the even-parity angular flux.

The above discussion shows a region-wise EPDF can be taken into by correction of cross sections, *i.e.*, the cross sections are divided by region-wise EPDF or are multiplied by the inverse of region-wise EPDF. In other words, a region-wise EPDF and the SPH factor can be used interchangeably. This is the straightforward extension of the relation between the region-wise DF and the SPH factor in diffusion theory. This discussion suggests that the region-wise EPDF can be estimated by an iteration procedure that is used for the SPH method. Once the SPH factor is obtained, the region-wise EPDF can be evaluated by:

$$\text{EPDF} = \frac{\phi^{\text{coarse}}}{\phi^{\text{fine}}} = \frac{1}{\text{SPH}}. \tag{8}$$

In this approach, only the region-average scalar flux is necessary, which is always edited in MOC calculations. Thus, existing MOC code can be directly used.

In Eq.(8), the region-wise scalar flux is used to estimate the angular independent region-wise EPDF. Since even parity angular flux is angular dependent, Eq.(8) can be extended to the angular dependent region-wise EPDF. In this case, region-average even-parity angular flux is used in Eq.(8) instead of the scalar fluxes. In the reference configuration, where EPDF is obtained, reaction rate and k-effective obtained by a fine calculation condition are reproduced both by the angular independent and the angular dependent region-wise EPDF. But in the case of "off-nominal" condition, *e.g.*, a colorset geometry, angular dependent region-wise EPDF would yield more robust and accurate results at the expense of computation time to tally the angular dependent even-parity angular flux and memory storage for the angular dependent EPDF. An in-depth investigation of this trade-off would be an interesting topic, but the angular independent EPDF is focused in this paper.

II.B. Implementation of EPDF for MOC

In diffusion theory (as well as the second-order Pn theory), the region-wise DF can be rigorously incorporated by dividing cross sections by DF when the discussion in section II.A is considered. However, this is not true for MOC, which utilizes the first order differential form. The difference between the diffusion and MOC comes from utilization of the diffusion coefficient (or the $1/\Sigma_t$ term) in these equations. Namely, in the diffusion equation, or the transport equation of second order form, both of Σ_t and $1/\Sigma_t$ explicitly

present, while only Σ_t appears in the transport equation of first order form [22]. In other words, an "additional type" of cross section $1/\Sigma_t$ is used in the diffusion and the transport theory of the second order differential form. Due to this additional freedom, the region-wise DF can be incorporated by dividing cross sections in the latter equations.

The even and odd parity angular fluxes at the interface are defined by the following angular flux definitions depicted in Fig.1:

$$\psi_L^e(\Omega) = \frac{\psi_{L,out}(\Omega) + \psi_{L,in}(-\Omega)}{2},$$

$$\psi_L^o(\Omega) = \frac{\psi_{L,out}(\Omega) - \psi_{L,in}(-\Omega)}{2},$$

$$\psi_R^e(\Omega) = \frac{\psi_{R,in}(\Omega) + \psi_{R,out}(-\Omega)}{2},$$
(9)

$$\psi_R^o(\Omega) = \frac{\psi_{R,in}(\Omega) - \psi_{R,out}(-\Omega)}{2},$$

where

$\psi_{L,out}(\Omega)$: the outgoing angular flux of region L,

$\psi_{L,in}(-\Omega)$: the incoming angular flux of region L,

$\psi_{R,in}(\Omega)$: the incoming angular flux of region R,

$\psi_{R,out}(-\Omega)$: the outgoing angular flux of region R.

To explicitly treat a region-wise EPDF in a transport calculation, the following conditions are used for the interface between the regions L and R.

$$f_L \psi_L^e = f_R \psi_R^e,$$
(10)

$$\psi_L^o = \psi_R^o,$$
(11)

where, f_L and f_R are the region-wise EPDF for the regions L and R, respectively.

Using Eqs. (10) and (11), the incoming angular flux from the region L to the region R is calculated by:

$$\psi_{R,in}(\Omega) = \frac{2f_L}{f_L + f_R} \psi_{L,out}(\Omega) + \frac{f_L - f_R}{f_L + f_R} \psi_{R,out}(-\Omega),$$
(12)

Utilization of Eq. (12) in MOC poses two issues. To calculate the incoming angular flux using Eq. (12), not only the outgoing angular flux from the region L ($\psi_{L,out}(\Omega)$), but also the outgoing angular flux from the region R ($\psi_{R,out}(-\Omega)$) are necessary. In common MOC transport sweeps, the incoming, the

outgoing, and the average angular fluxes on a segment of a ray trace are discarded once transport sweep is finished. This means that the outgoing angular flux from the region R ($\psi_{R,out}(-\Omega)$), which is the angular flux for opposite direction and is not usually preserved, is necessary. To resolve this issue, the transport sweep on a ray trace is iteratively carried out back and forth, *i.e.*, transport sweep on a ray trace is carried out for the forward direction, followed by the backward direction. Such transport sweep could be adopted to increase computational efficiency, *e.g.*, OpenMOC by MIT [23]. With this implementation, all incoming and outgoing angular fluxes on a ray trace can be preserved during transport sweep on this ray trace, and thus. Eq. (12) can be used. The preserved incoming and outgoing angular fluxes are discarded once transport sweep on a ray trace is finished.

Equation (12) indicates that an incoming angular flux is affected by the outgoing angular flux of opposite direction. Thus, iterations on a ray trace (back and forth iterations on a ray trace) are necessary to obtain converged angular fluxes, but the iteration is not necessary for the ordinary MOC transport sweep. The additional iterations on a ray trace have a negative impact on computational efficiency, but are adopted in the present study to verify the validity of the present method. For practical applications, a transport sweep algorithm would be changed, *e.g.*, directly solves even parity angular fluxes by the LU decomposition method and eliminate the necessity of iteration on a ray trace. This is a common practice of solving a finite-difference diffusion equation in one-dimensional geometry.

Extension to two- or three-dimensional geometry is straightforward since the even-parity transport equation on a ray trace is considered. Figure 2 depicts an example of an application in a two-dimensional geometry.

When Eq.(12) is used, the angular flux is discontinuous at the region boundary as shown in Fig.1. The partial current or the net current is edited from the angular flux for the acceleration calculation using the coarse mesh finite difference (CMFD) or the generalized coarse mesh rebalance (GCMR) method. The partial current and the net current should be calculated using the angular flux at the same region. For example, $\psi_{L,out}(\Omega) - \psi_{R,out}(-\Omega)$ cannot be used as the net neutron current. $\psi_{L,out}(\Omega) - \psi_{L,in}(-\Omega)$ or $\psi_{R,in}(\Omega) - \psi_{R,out}(-\Omega)$ should be used in Fig.1.

II.C. Estimation of EPDF through Iterations

The calculation procedures to estimate the region-wise angular-independent EPDF is summarized as follows:

(1) Perform a reference MOC transport calculation using a fine calculation condition.

(2) Save average scalar flux (ϕ^{fine} in Eq.(8)) in each flux region obtained in Step (1).

(3) Assume initial guess (1.0) of EPDF (EPDF in Eq.(8) or f_L, f_R in Eq.(12)) for all regions.

(4) Perform a MOC transport calculation using a coarse calculation condition considering EPDF using Eq. (14).

(5) Save the average scalar flux (ϕ^{coarse} in Eq.(8)) in each flux region obtained in Step (4).

(6) Estimate the region-wise EPDF using ϕ^{fine}, ϕ^{coarse}, and Eq.(8).

(7) Repeat Steps (4) to (6) until convergence.

The steps (1)-(7) are usually carried out in a single assembly geometry with the reflective boundary condition. In the present study, scalar flux is normalized as the volume integrated fission source over the whole geometry is 1.0. The steps (1)-(7) are exactly the same as that used to evaluate the SPH factor.

II.D. Normalization of EPDF using assembly discontinuity factor

As described in section II.C, region-wise EPDF is estimated in a single assembly geometry with the reflective boundary condition. Inconsistency between the fine and the coarse calculation results inside a single assembly is captured and corrected by the region-wise EPDF in each flux region. However, in a core or a colorset configuration, the discontinuity condition for the angular flux among different types of fuel assemblies should be also taken into account. In the advanced nodal method using the diffusion theory, this is incorporated by the assembly discontinuity factor (ADF). Similarly, discontinuity for even parity angular flux at assembly interface is taken into account by the assembly EPDF (AEPDF). Note that the AEPDF is not directly used in Eq.(12). Utilization of the AEPDF is described later. In the present study, AEPDF is calculated by:

$$\text{AEPDF} = \frac{\phi_{sur}^{\text{fine}}}{\phi_{sur,cor}^{\text{coarse}}}, \tag{13}$$

where ϕ_{sur}^{fine} and $\phi_{sur,cor}^{\text{coarse}}$ are the average surface scalar fluxes of fuel assembly obtained by the fine and the coarse calculation conditions. The subscript cor means that the correction (EPDF or SPH) is taken into account in the coarse calculation in Eq. (13). The definition of AEPDF given by Eq. (13) is the same as that of the conventional ADF.

Once AEPDF is obtained, it is used at the assembly boundary to correct discrepancy of angular flux levels among different fuel assemblies. Specifically, EPDFs obtained by the procedure shown in section II.C are multiplied by AEPDF. In the case of SPH method, the SPH factor in each flux region is divided by the AEPDF to correct the discrepancy, which is a straightforward extension of the improved SPH method or the Selengut normalization condition [24], [25]. The SPH factor is multiplied to the cross sections. Therefore, by dividing the SPH factor by ADF or AEPDF, ADF or AEPDF can be incorporated [25].

III. NUMERICAL RESULTS AND DISCUSSIONS

Two different configurations are considered in the verification calculations. The first one is the colorset geometries with the reflective boundary condition. The verification using the colorset configuration aims to confirm the validity of the present method in the low-leakage conditions with the reflective boundary. The second one is a small PWR core having baffle and reflector at the periphery, characterized by the higher leakage condition. The second verification indicates the performance of the present method in actual applications.

III.A. Colorset Calculations

III.A.1. Calculation conditions

The UOX2, UOX2 with BA, UOX2 with RCC, MOX1 fuel assemblies specified in the KAIST-2A benchmark problem [26] are used in the present study. Seven group cross sections for each material are given in the specifications. The region-wise EPDF, or the SPH factor, is evaluated in a single assembly geometry with the reflective boundary condition and then these correction factors are applied to the 2x2 colorset geometries shown in Fig.3, which represent typical conditions in LWRs.

Calculations are carried out by the GENESIS code in two-dimensional geometry. The GENESIS code is a transport code for two- or three-dimensional geometry [27], [28]. The conventional MOC method is used for two-dimensional geometries while the LEAF (Legendre polynomial Expansion of Angular Flux) method is used for three-dimensional geometries. In the present study, treatment of EPDF is implemented in the GENESIS code based on the algorithms described in section II.B for the test purpose. No optimization for computation time is considered during the present implementation, thus comparison of computation time is not carried out.

The EPDF can be used to capture the spatial, the angular, and the energetic discretization errors as described in Introduction. In the present study, we consider the spatial and angular discretization errors of ray traces in order to purely estimate the performance of the present method. Namely, the same number of energy groups and the background meshing are used for the coarse and fine calculation conditions. When the energy collapse is considered, correction on cross sections due to spectral interference among fuel assemblies should be taken into account. Similarly, in the case of homogenization, variation of the homogenized cross section due to adjacent fuel assembly should be considered. These considerations make a performance evaluation of the present method difficult. By using the simple calculation conditions, errors

11

due to these effects (energy collapsing, homogenization) can be neglected, which clarify the discussion on the performance of this method.

Calculation conditions for the GENESIS code are summarized as follows:

<Fine calculation condition>

•Number of flux regions in a cell: approximately 40 (see Fig.4)

•Ray trace width: 0.05 cm

•Number of azimuthal angles: 96 (for 2π)

•Number of polar angles: 3 (for $\pi/2$, the Tabuchi-Yamamoto quadrature set)

<Coarse calculation condition>

•Number of flux regions in a cell: approximately 40 (see Fig.4)

•Ray trace width: 0.1 cm

•Number of azimuthal angles: 8 (for 2π)

•Number of polar angles: 1 (for $\pi/2$, the Tabuchi-Yamamoto quadrature set)

Note that maximum and minimum values of the region-wise EPDF, or the SPH factor, are set to be 2.0 and 0.5, respectively, to avoid the numerical issue.

The verification is carried out by the following procedures:

(1) Perform single assembly calculations for UOX2, UOX2-BA, UOX2-RCC, and MOX1 using the fine calculation conditions

(2) Estimate the SPH factor or the region-wise EPDF for each flux region using the calculation procedure described in section II.C.

(3) Estimate AEPDF in each single fuel assembly and corrects the region-wise EPDF or the SPH factor by AEPDF for normalization as described in section II.D.

(4) Perform 2x2 colorset calculation using the fine calculation to obtain the reference solution

(5) Perform 2x2 colorset calculation using the coarse calculation condition. Calculations are carried out without any correction, with region-wise EPDF, or with the SPH factor.

(6) Compare the results obtained by Steps (4) and (5).

III.A.2. Numerical results and discussions

The region-wise EPDF, or the SPH factor, are obtained by the calculation procedure shown in section II.C. Convergence behaviors of the SPH factor and DF for the single assembly geometries are shown in Fig.5. Table I shows the maximum and the minimum values of the SPH factor and DF. No convergence problem is observed for EPDF and the obtained EPDFs are within the range of 0.5-2.0. However, in the case of SPH factor, the SPH factor reaches the upper or the lower limit in the case of UOX2-BA and UOX2-RCC. Note that BA indicates that Gd bearing fuel rods are used in the fuel assembly. If the range of the SPH factor is not limited, the SPH factor would be a very large or small value for these fuel assemblies.

K-effective, assembly-wise relative power, and pin-wise relative power in the 2x2 colorset geometries are compared. Table II summarizes the results of the comparison.

Table II indicates that the SPH method can improve prediction accuracy, especially assembly and pin-wise power distribution. The EPDF further improves assembly and pin-wise power distribution especially in the case of UOX2-UOX2BA and UOX2-UOX2RCC that contain strong neutron absorber. The SPH method with the normalization by AEPDF does not improve the prediction accuracy while the region-wise EPDF with the normalization by AEPDF further improves accuracy for all cases.

Comparison of pin-wise power distribution for the case of UOX2-UOX2BA is shown in Fig.6. By using the region-wise EPDF with normalization, coarse calculation well reproduces the reference result. In the present study, the improved SPH method, *i.e.*, the normalization of the SPH factors using AEPDF, does not contribute to accuracy improvement. The improved SPH method, which is equivalent to the SPH with AEPDF normalization, has been used with the simplified Pn theory. In the case of SPn method, the improved SPH method can reduce the error of pin-wise power distribution as shown in reference [25]. Reference [20] also describes the importance of normalization, which improves the accuracy. The difference between the references [20], [25] and the current study would come from the fact that the SPH correction is different between the SPn method and MOC as discussed in the reference [22]. However, the in-depth investigation will be desirable to fully address this issue.

III.B. Core calculation

III.B.1. Calculation conditions

A small PWR core specified in the KAIST-2A benchmark problem is used as the second verification geometry. The UOX1, UOX2, UOX2 with BA, MOX1, and MOX1-BA fuel assemblies specified in the KAIST benchmark are used with the baffle-reflector and reflector assemblies. Note that the thickness of baffle is 2.52 cm, which corresponds to the pitch of two cells. Calculation geometry is shown in Fig.7.

Calculations are carried out by the GENESIS code using the MOC option in two-dimensional geometry as described in section III.A. Other calculation conditions are summarized as follows:

<Fine calculation condition>

•Number of flux regions in a fuel cell: approximately 40 (see Fig.4)

•Number of flux regions in a reflector cell: 36

•Ray trace width: 0.05 cm

•Number of azimuthal angles: 96 (for 2π)

•Number of polar angles: 3 (for $\pi/2$, the Tabuchi-Yamamoto quadrature set)

<Coarse calculation condition>

•Number of flux regions in a cell: approximately 40 (see Fig.4)

•Number of flux regions in a reflector cell: 36

•Ray trace width: 0.1 cm

•Number of azimuthal angles: 8 (for 2π)

•Number of polar angles: 1 (for $\pi/2$, the Tabuchi-Yamamoto quadrature set)

Corrections by EPDF or SPH are considered only for the fuel assemblies. No correction is taken into account at the baffle-reflector and the reflector assemblies even in the case of coarse calculation condition. Maximum and minimum values of the region-wise EPDF or the SPH factor are set to be 2.0 and 0.5. The verification procedures are identical to those described section III.A.

III.B.2. Numerical results and discussions

Summary of calculation results is shown in Table III. The error of pin power distribution is shown in Fig.8 for four cases (SPH, SPH with AEPDF normalization, EPDF, and EPDF with AEPDF normalization). Table III indicates that reduction of discretization error by the SPH and EPDF without the normalization is marginal in the core calculation. Since various fuel assemblies with different heterogeneity exist in the core, normalization by AEPDF is important. By comparing the results of EPDF and EPDF with the normalization shown in Fig.8, the EPDF with normalization can offset systematic discrepancies among fuel assemblies. This indicates the effectiveness of the normalization.

Though no correction is considered in the baffle-reflector and reflector assemblies, EPDF with normalization gives significant improvement both for the assembly power and pin power distributions. Not

only the maximum and minimum errors but also the root mean square error are reduced using the EPDF with normalization. On the contrary, the SPH correction with normalization gives worse results than other cases. This is consistent with the results obtained in 2x2 colorset calculations.

IV. CONCLUSIONS

In the present study, the region-wise discontinuity factor for even parity angular flux (EPDF) is used to correct discretization error due to coarse calculation condition of MOC. An iterative procedure using only region-wise scalar flux is adopted to estimate EPDF.

The present method is applied to the 2x2 colorset and the core benchmark problems whose specification is taken from the KAIST-2A benchmark. Calculation results indicate that the present method using the region-wise EPDF shows better results than those with the conventional SPH method. Convergence issues in the estimation of the EPDFs were not observed. The calculation results show that the region-wise EPDF can well capture discretization error caused by a coarse calculation condition in the colorset and core geometries.

There are several issues to be addressed regarding this work. At first, an efficient MOC sweep algorithm with EPDF is desirable for practical applications. Since EPDF is applied to the even parity angular flux, a dedicated solver to handle the transport equation of second-order differential form may be necessary. Next, the region-wise EPDF is incorporated through discontinuity of angular flux in this study. However, if the region-wise EPDF can be taken into account through correction of cross sections, additional implementation work is not necessary for existing MOC codes. Previous work reveals that EPDF can be explicitly considered by additional anisotropic scattering component [22]. Example of equivalence between EPDF and SPH with anisotropic scattering is shown in Appendix A. However since the use of anisotropic scattering cross section requires larger computational resources (from the viewpoint of computation time and memory storage), an alternate method without correction of anisotropic scattering is desirable.

REFERENCES

1. J. Y. CHO et al., "Three-Dimensional Heterogeneous Whole Core Transport Calculation Employing

Planar MOC Solutions," *Trans. Am. Nucl. Soc.*, **87**, 234 (2002).

2. S. KOSAKA and T. TAKEDA, "Verification of 3D Heterogeneous Core Transport Calculation Utilizing NonLinear Iteration Technique," *J. Nucl. Sci. Technol.*, **41**, 645 (2004).

3. H. G. JOO et al., "Methods and Performance of a Three Dimensional Whole-Core Transport Code DeCART," *Proc. PHYSOR 2004*, Chicago, Illinois, April 25–29, 2004, American Nuclear Society (2004). [CD-ROM]

4. B. KOCHUNAS et al., "Overview of Development and Design of MPACT: Michigan Parallel Characteristics Transport Code," *Proc. M&C 2013*, Sun Valley, Idaho, May 5–9, 2013, American Nuclear Society (2013). [USB-DRIVE]

5. Y. S. JUNG et al., "Practical Numerical Reactor Employing Direct Whole Core Neutron Transport and Subchannel Thermal/Hydraulic Solvers," *Ann. Nucl. Energy*, **62**, 357 (2013).

6. M. RYU et al., "Solution of the BEAVRS Benchmark Using the nTRACER Direct Whole Core Calculation Code," *J. Nucl. Sci. Technol.*, **52**, 961 (2015).

7. A. KAVENOKY, "The SPH homogenizaion method," Proceedings of Meeting Homogenization Methods in Reactor Physics, Guano, Switzerland, IAEA-TECDOC-231, (1980).

8. A. HEBERT, "A Consistent Technique for the Pin-by-pin Homogenization of a Pressurized Water Reactor Assembly," *Nucl. Sci. Eng.* **113**, 227 (1991).

9. A. HEBERT, G. MATHONNIERE, "Development of a Third-generation Superhomogeneisation Method for the Homogenization of a Pressurized Water Reactor Assembly," *Nucl. Sci. Eng.*, **115**, 129 (1993).

10. M. TATSUMI, A. YAMAMOTO, "Advanced PWR Core Calculation Based on Multi-group Nodal-transport Method in Three-dimensional Pin-by-Pin Geometry," *J. Nucl. Sci. Technol.*, **40**, 376 (2003).

11. N. SUGIMURA, A. YAMAMOTO, "Resonance Treatment Based on Ultra-fine-group Spectrum Calculation in the AEGIS Code," *J. Nucl. Sci. Technol.*, **44**, 958 (2007).

12. H. PARK, H. G. JOO, "Practical Resolution of Angle Dependency of Multigroup Resonance Cross Sections using Parametrized Spectral Superhomogenization Factors," *Nucl. Eng. Technol.*, **49**, 1287 (2017).

13. K. KOEBKE, "A New Approach to Homogenization and Group Condensation," Proceedings of IAEA Technical Committee Meeting on Homogenization Methods in Reactor Physics, Lugano, Switzerland, (1978).

14. K. S. SMITH, "Assembly Homogenization Techniques for Light Water Reactor Analysis," *Prog. Nucl. Energy*, **17**, 303 (1986).

15. R. SANCHEZ, "Assembly Homogenization Techniques for Core Calculations," *Prog. Nucl. Energy*, **51** 14 (2009).

16. T. SAKAMOTO, T. ENDO, A. YAMAMOTO, "Applicability of Angular Flux Discontinuity Factor Preserving Region-wise Leakage for Integro-differential Transport Equation," *J. Nucl. Sci. Technol.* **51**, 1264 (2014).

17. J. Y. CHO, H. G. JOO, S. Y. PARK, S. Q. ZEE, "Consistent Group Collapsing Scheme for Multi-group MOC Calculation," Proc. PHYSO2002, Seoul, Korea, Oct.7-10, 2002, American Nuclear Society (2002) [CD-ROM].

18. G. GIUDICELLI, K. SMITH, B. FORGET, "Generalized Equivalence Methods for 3D Multigroup Neutron Transport." Ann. Nucl. Energy, **112**, 9 (2018).

19. A. YAMAMOTO, T. ENDO, Y. A. CHAO, "A Derivation of Discontinuity Factor for Angular Flux in Integrodifferential Transport Equation," *Trans. Am. Nucl. Soc.*, **104**, 815 (2011).

20. L. YU, Y. A. CHAO, "A Unified Generic Theory on Discontinuity Factors in Diffusion, SP3 and Transport Calculations," *Ann. Nucl. Energy*, **75**, 239 (2015).

21. E. E. LEWIS, W. F. MILLER, Computational Methods of Neutron Transport, Chap.6, John Wiley & Sons, ISBN 0-471-09245-2 (1984).

22. A. YAMAMOTO, "Utilization of Discontinuity Factor in Integro-differential Type of Boltzmann Transport Equation," Proceedings of International Conference on Physics of Reactors (PHYSOR2010), Pittsburgh, USA, (2010). [CD-ROM]

23. W. BOYD, S. SHANER, L. LI, B. FORGET, K. SMITH, "The OpenMOC Method of Characteristics Neutral Particle Transport Code." Ann. Nucl. Energy, **68**, 43 (2014). (or https://mit-crpg.github.io/OpenMOC/methods/eigenvalue_calculations.html#transport-sweep-algorithm)

24. D. S. SELENGUT, "Diffusion Coefficients for Heterogeneous Systems," *Trans. Am. Nucl. Soc.*, **3** 398 (1960).

25. A. YAMAMOTO, M. TATSUMI, Y. KITAMURA, AND Y. YAMANE, "Improvement of the SPH Method for Pin-by-pin Core Calculations," *J. Nucl. Sci. Technol.*, **41**, 1155 (2004).

26. N. Z. CHO, *Benchmark Problems in Reactor and Particle Transport Physics*, KAIST, (2000).

27. A. YAMAMOTO, A. GIHO, Y. KATO, T. ENDO, "GENESIS – A Three-dimensional Heterogeneous Transport Solver based on the Legendre Polynomial Expansion of Angular Flux Method," *Nucl. Sci. Eng*, **1**, 186 (2017).

28. A. YAMAMOTO, A. GIHO, T. ENDO, "Recent Developments in the GENESIS Code based on the LEAF Method," *Nucl. Eng Technol.*, https://doi.org/10.1016/j.net.2017.06.016 (2017).

APPENDIX A

MOC calculations using the following four cross sections are compared for the MOX1 single fuel assembly used in the verification calculation: (1) Original cross section with EPDF, (2) Original (not corrected) cross section without EPDF, (3) SPH corrected P0 cross section, (4) SPH corrected P7 cross section. Note that in Cases (3) and (4), the inverse of the EPDF used in Case (1) is directly used as the SPH factor. Case (3) is equivalent to the conventional SPH correction. Case (4) includes additional anisotropic scattering cross sections (up to P7 here) to make Cases (1) and (4) equivalent. See Eq.(25) in reference [13] for detail.

Calculation conditions for the GENESIS code are as follows: 48 azimuthal angle divisions for 2π, 8 polar angle divisions for π with the Gauss-Legendre quadrature set, 0.1 cm ray trace width.

Calculation results are shown in Fig. A-1. Figure A-1 indicates that Case (4) reproduces Case (1). The slight difference observed in Case (4) comes from the spatial and angular discretization errors.

List of Tables

List of Figures

Table I. Maximum and minimum values of the SPH factor and DF for the 2x2 colorset geometry

		Fuel assembly type			
		UOX2	MOX1	UOX2-BA	UOX2-RCC
Maximum	SPH	1.086	1.095	2.000	2.000
	DF	1.056	1.149	1.082	1.212
Minimum	SPH	0.947	0.840	0.500	0.500
	DF	0.920	0.912	0.892	0.899

Table II. Summary of calculation results for 2x2 colorset calculations

Configuration	Azimuthal (2π)	Polar (0.5π)	Ray width (cm)	Correction	Normalization	Keffective		Assembly power				Pin power				Difference of pin powers		
						Keffective	Difference (%)	UOX2	Difference (%)	Other	Difference (%)	Maximum pin power	Difference (%)	Minimum pin power	Difference (%)	Maximum (%)	Minimum (%)	RMS (%)
UOX2-UOX2RCC	96	3	0.05	Ref.	---	1.08384		361.52		166.48		1.7272		0.3968				
	8	1	0.10	No	No	1.08395	0.010	364.20	0.74	163.80	-1.61	1.7539	1.55	0.3875	-2.35	1.55	-4.17	1.60
	8	1	0.10	SPH	No	1.08476	0.085	363.09	0.43	164.91	-0.94	1.7390	0.68	0.3898	-1.77	0.74	-1.93	0.86
	8	1	0.10	EPDF	No	1.08497	0.104	362.48	0.27	165.52	-0.58	1.7338	0.38	0.3923	-1.14	0.45	-1.24	0.54
	8	1	0.10	SPH	Yes (w/AEPDF)	1.09105	0.666	364.36	0.79	163.64	-1.71	1.7580	1.78	0.3803	-4.18	1.81	-4.28	1.78
	8	1	0.10	EPDF	Yes (w/AEPDF)	1.08451	0.062	361.92	0.11	166.08	-0.24	1.7318	0.27	0.3939	-0.74	0.49	-0.83	0.31
UOX2-UOX2BA	96	3	0.05	Ref.	---	1.15982		311.68		216.32		1.3591		0.0813				
	8	1	0.10	No	No	1.16059	0.066	312.58	0.29	215.43	-0.41	1.3702	0.82	0.0816	0.39	1.04	-1.86	0.53
	8	1	0.10	SPH	No	1.16001	0.016	312.50	0.26	215.50	-0.38	1.3649	0.43	0.0809	-0.49	0.45	-0.71	0.36
	8	1	0.10	EPDF	No	1.16009	0.023	312.23	0.18	215.77	-0.25	1.3629	0.28	0.0810	-0.26	0.29	-0.49	0.25
	8	1	0.10	SPH	Yes (w/AEPDF)	1.16227	0.211	313.49	0.58	214.51	-0.83	1.3780	1.39	0.0792	-2.56	1.39	-2.59	0.94
	8	1	0.10	EPDF	Yes (w/AEPDF)	1.15995	0.011	311.87	0.06	216.13	-0.09	1.3611	0.15	0.0812	-0.02	0.41	-0.26	0.12
UOX2-MOX1	96	3	0.05	Ref.	---	1.21331		272.30		255.70		1.1908		0.6797				
	8	1	0.10	No	No	1.20932	-0.329	275.07	1.01	252.93	-1.08	1.2125	1.82	0.6628	-2.49	1.82	-2.49	1.21
	8	1	0.10	SPH	No	1.21340	0.008	273.09	0.29	254.91	-0.31	1.1934	0.22	0.6778	-0.27	0.60	-1.12	0.35
	8	1	0.10	EPDF	No	1.21340	0.007	273.13	0.31	254.87	-0.33	1.1933	0.21	0.6779	-0.27	0.68	-0.98	0.36
	8	1	0.10	SPH	Yes (w/AEPDF)	1.21313	-0.015	274.25	0.72	253.75	-0.76	1.2012	0.87	0.6743	-0.79	1.16	-1.46	0.78
	8	1	0.10	EPDF	Yes (w/AEPDF)	1.21333	0.002	272.87	0.21	255.13	-0.22	1.1947	0.33	0.6772	-0.38	0.41	-0.38	0.26

Table III. Summary of calculation results for core calculation

Configuration	Azimuthal (2π)	Polar (0.5π)	Ray width (cm)	Correction	Normalization	Keffective	Keffective Difference (%)	Difference of assembly powers			Difference of pin powers		
								Maximum (%)	Minimum (%)	RMS (%)	Maximum (%)	Minimum (%)	RMS (%)
KAIST 2A	96	3	0.05	Ref.	---	1.13511							
	8	1	0.10	No	No	1.13450	0.01	0.96	-1.28	0.80	2.38	-4.72	1.09
	8	1	0.10	SPH	No	1.13685	0.08	0.49	-0.94	0.49	1.00	-5.65	0.96
	8	1	0.10	EPDF	No	1.13663	0.10	0.47	-0.76	0.41	0.99	-5.07	0.84
	8	1	0.10	SPH	Yes (w/AEPDF)	1.14036	0.67	1.44	-2.99	1.63	2.25	-11.01	2.56
	8	1	0.10	EPDF	Yes (w/AEPDF)	1.13676	0.06	0.62	-0.25	0.27	1.51	-0.60	0.34
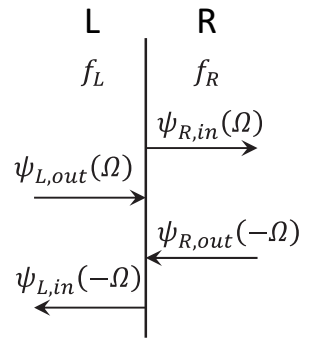
Figure 1. Discontinuity of angular flux at an interface using EPDF
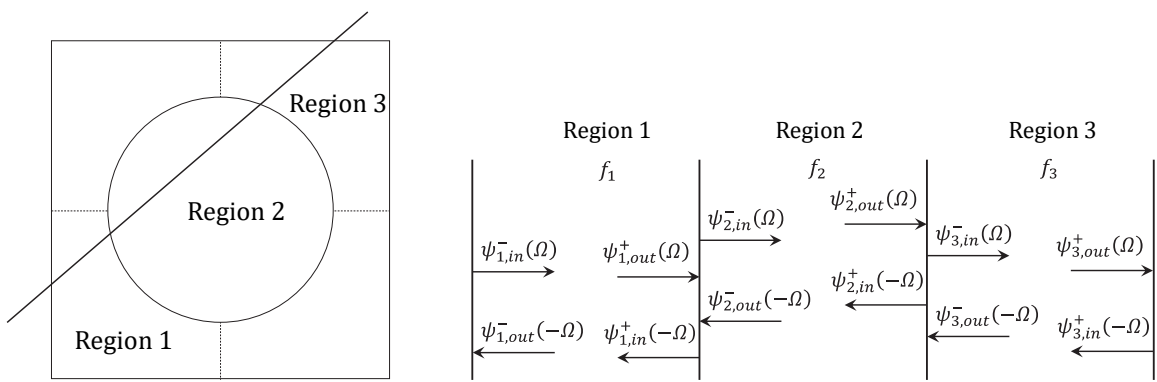
Figure 2. Application of EPDF to a ray trace in a two-dimensional geometry

UOX2	UOX2-RCC
UOX2-RCC	UOX2

UOX2	UOX2-BA
UOX2-BA	UOX2

UOX2	MOX1
MOX1	UOX2

Figure 3. 2x2 colorset geometries
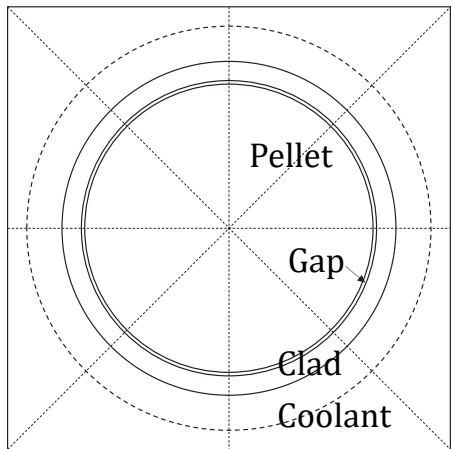
Figure 4. Background meshing in a fuel cell in KAIST-2A benchmark problem
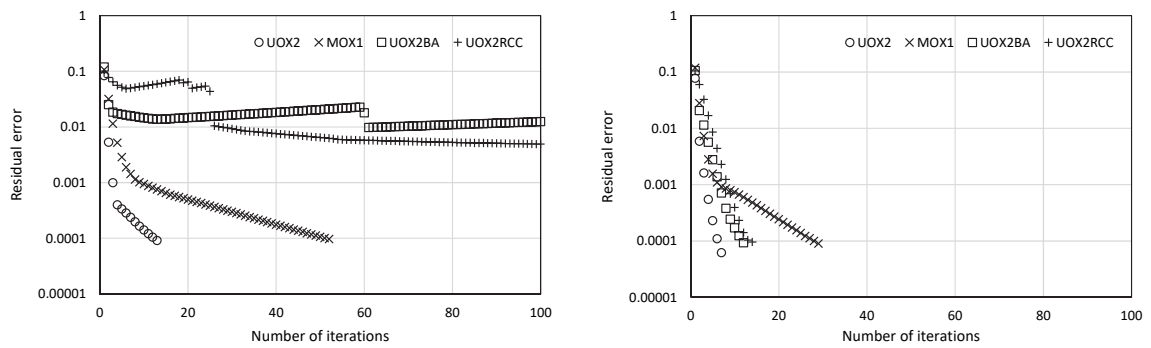
Figure 5. Convergence behaviors of the SPH factor (left) and DF (right) in single assembly geometry

3.0%
2.0%
1.0%
0.0%
-1.0%
-2.0%
-3.0%

SPH without normalization by AEPDF

EPDF without normalization by AEPDF

SPH with normalization by AEPDF

EPDF with normalization by AEPDF
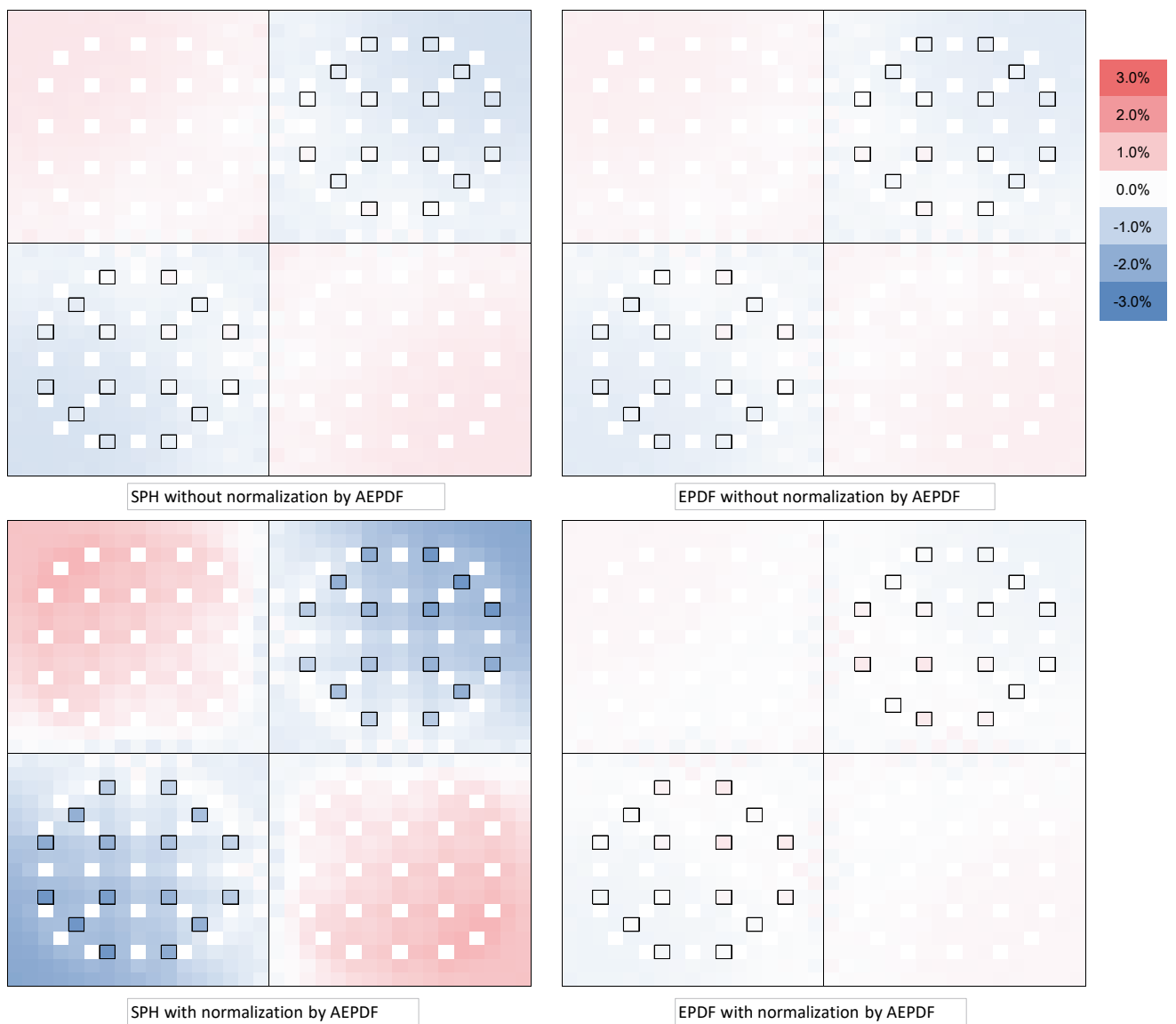
Figure 6. Comparison of pin-wise error for the UOX2-UOX2BA colorset configuration. The Gd bearing fuel rods are indicated by the black rectangle around fuel pin.

(Color production desired)

Baffle-reflector	Baffle-reflector	Baffle-reflector	Reflector	Reflector
UOX1	UOX1	Baffle-reflector	Baffle-reflector	Reflector
MOX1	UOX2	UOX1	Baffle-reflector	Baffle-reflector
UOX2	MOX1-BA	UOX2	UOX1	Baffle-reflector
UOX2-BA	UOX2	MOX1	UOX1	Baffle-reflector

C̶L

C̶L

Figure 7. KAIST-2A core geometry

SPH without normalization by AEPDF

EPDF without normalization by AEPDF

SPH with normalization by AEPDF

EPDF with normalization by AEPDF
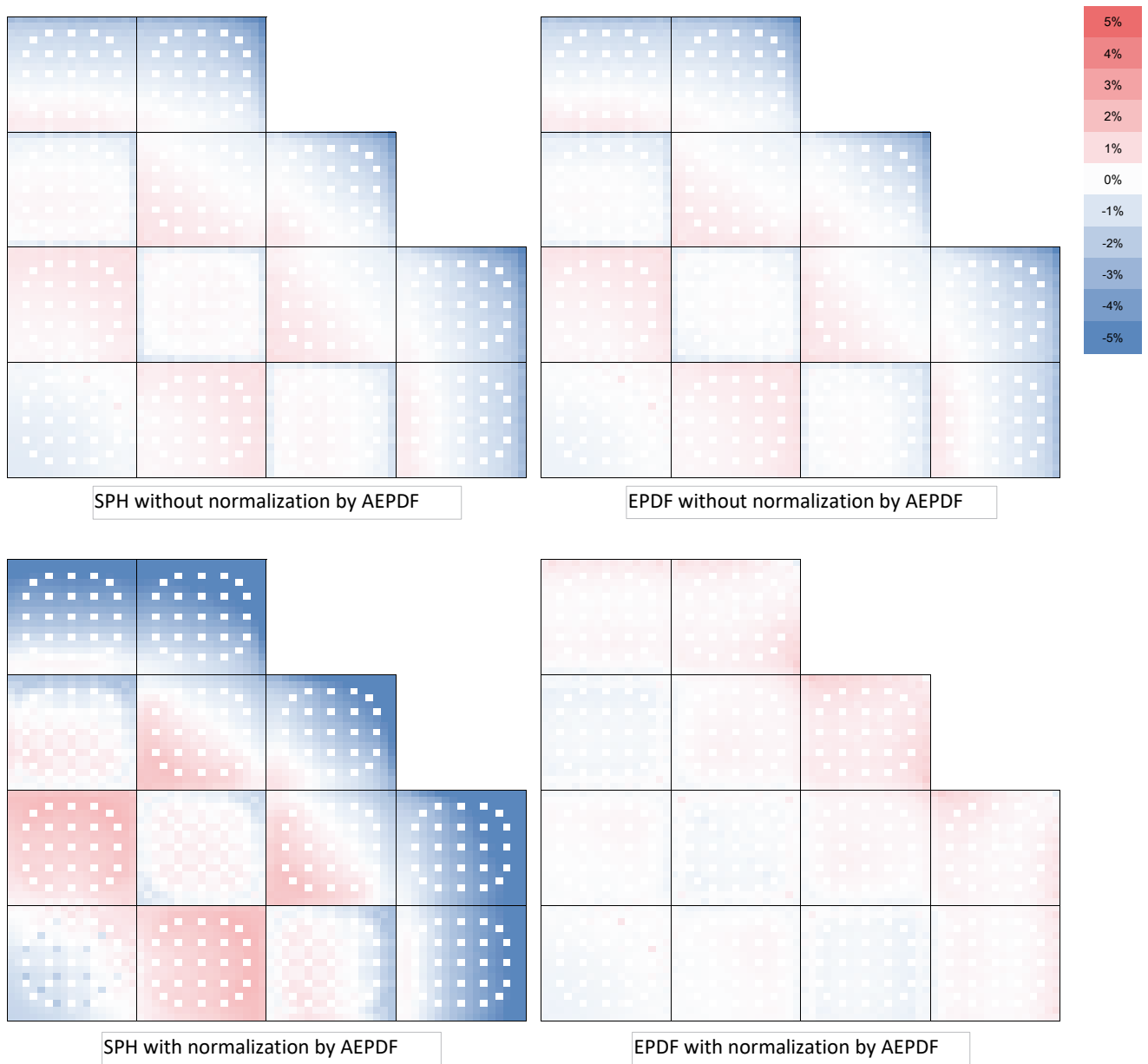
Figure 8. Comparison of pin-wise error for the KAIST-2A core configuration.

(Color production desired)

Case | **Difference of k-infinity** | Difference of pin-wise fission rate from Case (1) [Original P0 cross section with EPDF, reference]

Case (2) — Original P0 cross section with EPDF — Difference of k-infinity: -0.71%

|																
-0.05	0.27	-0.12	-0.40	0.54	-0.28	0.24	0.25	0.11	0.25	0.24	-0.28	0.54	-0.40	-0.12	0.27	-0.05
0.27	-0.66	0.33	0.43	0.07	-0.01	0.49	-0.25	-0.10	-0.25	0.49	-0.01	0.07	0.43	0.33	-0.66	0.27
-0.12	0.33	-0.09	0.10	-0.12		0.12	-0.28		-0.28	0.12		-0.12	0.10	-0.09	0.33	-0.12
-0.40	0.43	0.10		0.26	0.08	-0.20	-0.10	0.21	-0.10	-0.20	0.08	0.26		0.10	0.43	-0.40
0.54	0.07	-0.12	0.26	-0.37	0.32	0.35	-0.31	-0.52	-0.31	0.35	0.32	-0.37	0.26	-0.12	0.07	0.54
-0.28	-0.01		0.08	0.32		0.05	-0.09		-0.09	0.05		0.32	0.08		-0.01	-0.28
0.24	0.49	0.12	-0.20	0.35	0.05	-0.37	-0.23	-0.47	-0.23	-0.37	0.05	0.35	-0.20	0.12	0.49	0.24
0.25	-0.25	-0.28	-0.10	-0.31	-0.09	-0.23	0.01	-0.52	0.01	-0.23	-0.09	-0.31	-0.10	-0.28	-0.25	0.25
0.11	-0.10		0.21	-0.52		-0.47	-0.52		-0.52	-0.47		-0.52	0.21		-0.10	0.11
0.25	-0.25	-0.28	-0.10	-0.31	-0.09	-0.23	0.01	-0.52	0.01	-0.23	-0.09	-0.31	-0.10	-0.28	-0.25	0.25
0.24	0.49	0.12	-0.20	0.35	0.05	-0.37	-0.23	-0.47	-0.23	-0.37	0.05	0.35	-0.20	0.12	0.49	0.24
-0.28	-0.01		0.08	0.32		0.05	-0.09		-0.09	0.05		0.32	0.08		-0.01	-0.28
0.54	0.07	-0.12	0.26	-0.37	0.32	0.35	-0.31	-0.52	-0.31	0.35	0.32	-0.37	0.26	-0.12	0.07	0.54
-0.40	0.43	0.10		0.26	0.08	-0.20	-0.10	0.21	-0.10	-0.20	0.08	0.26		0.10	0.43	-0.40
-0.12	0.33	-0.09	0.10	-0.12		0.12	-0.28		-0.28	0.12		-0.12	0.10	-0.09	0.33	-0.12
0.27	-0.66	0.33	0.43	0.07	-0.01	0.49	-0.25	-0.10	-0.25	0.49	-0.01	0.07	0.43	0.33	-0.66	0.27
-0.05	0.27	-0.12	-0.40	0.54	-0.28	0.24	0.25	0.11	0.25	0.24	-0.28	0.54	-0.40	-0.12	0.27	-0.05

Case (3) — SPH corrected P0 cross section — Difference of k-infinity: 0.02%

-0.09	-0.08	-0.15	-0.18	-0.03	-0.19	-0.09	-0.10	-0.16	-0.10	-0.09	-0.19	-0.03	-0.18	-0.15	-0.08	-0.09
-0.08	-0.17	0.19	0.16	0.07	0.07	0.12	0.00	0.10	0.00	0.12	0.07	0.07	0.16	0.20	-0.17	-0.08
-0.15	0.19	0.03	0.04	-0.14		-0.01	-0.07		-0.07	-0.01		-0.14	0.04	0.03	0.20	-0.15
-0.18	0.16	0.04		-0.11	-0.01	-0.04	-0.07	-0.03	-0.07	-0.04	-0.01	-0.11		0.04	0.16	-0.18
-0.03	0.07	-0.14	-0.11	-0.14	0.25	0.22	0.00	-0.04	0.00	0.22	0.25	-0.14	-0.11	-0.14	0.07	-0.03
-0.19	0.07		-0.01	0.25		0.06	0.11		0.11	0.06		0.25	-0.01		0.07	-0.19
-0.09	0.12	-0.01	-0.04	0.22	0.06	0.03	0.01	-0.14	0.01	0.03	0.06	0.22	-0.04	-0.01	0.12	-0.09
-0.10	0.00	-0.07	-0.07	0.00	0.11	0.01	0.03	-0.06	0.03	0.01	0.11	0.00	-0.07	-0.07	0.00	-0.10
-0.16	0.10		-0.03	-0.04		-0.14	-0.06		-0.06	-0.14		-0.04	-0.03		0.10	-0.16
-0.10	0.00	-0.07	-0.07	0.00	0.11	0.01	0.03	-0.06	0.03	0.01	0.11	0.00	-0.07	-0.07	0.00	-0.10
-0.09	0.12	-0.01	-0.04	0.22	0.06	0.03	0.01	-0.14	0.01	0.03	0.06	0.22	-0.04	-0.01	0.12	-0.09
-0.19	0.07		-0.01	0.25		0.06	0.11		0.11	0.06		0.25	-0.01		0.07	-0.19
-0.03	0.07	-0.14	-0.11	-0.14	0.25	0.22	0.00	-0.04	0.00	0.22	0.25	-0.14	-0.11	-0.14	0.07	-0.03
-0.18	0.16	0.04		-0.11	-0.01	-0.04	-0.07	-0.03	-0.07	-0.04	-0.01	-0.11		0.04	0.16	-0.18
-0.15	0.20	0.03	0.04	-0.14		-0.01	-0.07		-0.07	-0.01		-0.14	0.04	0.03	0.19	-0.15
-0.08	-0.17	0.20	0.16	0.07	0.07	0.12	0.00	0.10	0.00	0.12	0.07	0.07	0.16	0.19	-0.17	-0.08
-0.09	-0.08	-0.15	-0.18	-0.03	-0.19	-0.09	-0.10	-0.16	-0.10	-0.09	-0.19	-0.03	-0.18	-0.15	-0.08	-0.09

Case (4) — SPH corrected P7 cross section — Difference of k-infinity: 0.01%

-0.02	-0.02	-0.04	-0.05	-0.02	-0.05	-0.02	-0.03	-0.05	-0.03	-0.02	-0.05	-0.02	-0.05	-0.04	-0.02	-0.02
-0.02	-0.04	0.04	0.02	0.03	0.02	0.04	0.02	0.02	0.02	0.04	0.02	0.03	0.02	0.04	-0.04	-0.02
-0.04	0.04	0.01	0.00	-0.01		0.00	-0.03		-0.03	0.00		-0.01	0.00	0.01	0.04	-0.04
-0.05	0.02	0.00		0.00	-0.02	0.00	-0.01	-0.02	-0.01	0.00	-0.03	0.00		0.00	0.02	-0.05
-0.02	0.03	-0.01	0.00	-0.01	0.05	0.05	0.01	-0.02	0.01	0.05	0.05	-0.01	0.00	-0.01	0.03	-0.02
-0.05	0.02		-0.02	0.05		0.00	0.00		0.00	0.00		0.05	-0.03		0.02	-0.05
-0.02	0.04	0.00	0.00	0.05	0.00	0.01	0.02	-0.04	0.02	0.01	0.00	0.05	0.00	0.00	0.04	-0.02
-0.03	0.02	-0.03	-0.01	0.01	0.00	0.02	0.03	-0.03	0.03	0.02	0.00	0.01	-0.01	-0.03	0.02	-0.03
-0.05	0.02		-0.02	-0.02		-0.04	-0.03		-0.03	-0.04		-0.02	-0.02		0.02	-0.05
-0.03	0.02	-0.03	-0.01	0.01	0.00	0.02	0.03	-0.03	0.03	0.02	0.00	0.01	-0.01	-0.03	0.02	-0.03
-0.02	0.04	0.00	0.00	0.05	0.00	0.01	0.02	-0.04	0.02	0.01	0.00	0.05	0.00	0.00	0.04	-0.02
-0.05	0.02		-0.03	0.05		0.00	0.00		0.00	0.00		0.05	-0.02		0.02	-0.05
-0.02	0.03	-0.01	0.00	-0.01	0.05	0.05	0.01	-0.02	0.01	0.05	0.05	-0.01	0.00	-0.01	0.03	-0.02
-0.05	0.02	0.00		0.00	-0.03	0.00	-0.01	-0.02	-0.01	0.00	-0.02	0.00		0.00	0.02	-0.05
-0.04	0.04	0.01	0.00	-0.01		0.00	-0.03		-0.03	0.00		-0.01	0.00	0.01	0.04	-0.04
-0.02	-0.04	0.04	0.02	0.03	0.02	0.04	0.02	0.02	0.02	0.04	0.02	0.03	0.02	0.04	-0.04	-0.02
-0.02	-0.02	-0.04	-0.05	-0.02	-0.05	-0.02	-0.03	-0.05	-0.03	-0.02	-0.05	-0.02	-0.05	-0.04	-0.02	-0.02

Figure A-1. Comparison of k-infinity and pin-wise fission rate for MOX1 fuel assembly

(Color production desired)